Journal of Solid State Chemistry 239 (2016) 228–236

Contents lists available at ScienceDirect

Journal of Solid State Chemistry

journal homepage: www.elsevier.com/locate/jssc

Insights into stability, electronic properties, defect properties and Li ions migration of Na, Mg and Al-doped $LiVPO_4F$ for cathode materials of lithium ion batteries: A first-principles investigation

Xiaojun Lv [a], Zhenming Xu [a], Jie Li [a,*], Jiangan Chen [b], Qingsheng Liu [c]

[a] School of Metallurgy and Environment, Central South University, Changsha 410083, China
[b] Faculty of Resource and Environmental Engineering, Jiangxi University of Science and Technology, Ganzhou 341000, China
[c] Faculty of Metallurgical and Chemical Engineering, Jiangxi University of Science and Technology, Ganzhou 341000, China

ARTICLE INFO

Article history:
Received 6 February 2016
Received in revised form
20 April 2016
Accepted 1 May 2016
Available online 2 May 2016

Keywords:
First-principles
$LiVPO_4F$
Doping
Electrical conductivity
Li ions migration

ABSTRACT

The effects of Na, Mg and Al doping on the structure, electronic property, defect property and Li ions migration of $LiVPO_4F$ were investigated by the first-principles method. Calculations show that the processes of forming $Li_{0.875}Na_{0.125}VPO_4F$, α- and β-$LiMg_{0.375}V_{0.75}PO_4F$, α- and β-$LiAl_{0.125}V_{0.875}PO_4F$ are all feasible. Na, Mg and Al doping significantly improve the electrical conductivity of $LiVPO_4F$ and simultaneously maintain their structural stability attributing to the reduction of band gaps through variations of V-3*d* spin up orbitals. Li vacancy defects of $LiVPO_4F$ are not ignorable, and vacancy defects with a lower activation energy for Li atom are far more likely to occur than Frenkel defects for Li and vacancy defects for other atoms. For pristine $LiVPO_4F$, path D along [0.012 0.$\bar{1}$7 0.572] direction is found to have the lowest activation energy of 0.418 eV, suggesting that anisotropic nature of Li ion conduction and $LiVPO_4F$ is a one-dimensional (1D)-ion conductor. The corresponding diffusion coefficient was estimated to be 2.82×10^{-9} cm^2/s, which is in good agreement with those experimental values.

1. Introduction

Lithium ion batteries have been widely applied in the field of portable energy storage because of their advantages of high voltage, high energy density, long cycle life and environmental friendliness [1–5]. Choosing appropriate electrode materials is a key factor in the production of high-performance lithium ion batteries. The $LiMO_2$ family (M=Co, Mn, Ni) is currently the dominant class of commercial cathode materials for lithium ion batteries [2,6–9]. To overcome the shortage of former $LiMO_2$ (M=Co, Mn, Ni), much effort has been directed towards the search for new cathode and anode materials with advantages of higher energy density, longer cycle life, and lower cost [10–19]. Among many cathode materials, $LiVPO_4F$ materials have become the promising candidates for next-generation lithium-ion batteries [14,17–21]. Compared to the corresponding oxide systems, $LiVPO_4F$ materials phosphate series generate a higher voltage of 4.2 V, and have higher energy density, better thermodynamic stability and better electrochemical properties, resulting of the substitution of oxygen ions by fluorophosphate groups arousing lager improvement of stability of three-dimensional structure. Barker et al. have firstly prepared the $LiVPO_4F$ materials by means of CTR (carbothermal reduction), with a specific capacity of 135 and 115 mAh g^{-1} for charge and discharge, Coulombic efficiency of 84% and a stable discharge platform 4.17 V [17–20].

To further improve the capacity and conductivity of $LiVPO_4F$ material, many recent experimental studies have been carried out by means of Al [22,23], Y [24], Na [25]and Ti [26] doping, and experimental results show that doping can enhance the thermodynamic stability and electrochemical properties such as cycle ability and electric capacity. For doping metal ions, more and more experimental efforts have been made, but for the study of theoretical mechanism for ion doping in $LiVPO_4F$ material is relatively less. Lack of corresponding theoretical explanations on their excellent performances, our knowledge of the influence of ion doping on crystal structure, electronic properties, defect properties and Li ions migration is superficial. Meanwhile, molecular simulation techniques such as electronic structure methods based on density functional theory (DFT), and atomistic potentials-based methods provide us with powerful instruments to predict the structure, defect chemistry, charge distributions and band structures, and kinetic studies of lithium ion diffusion processes, which can provide atomic understanding of the capacity, reaction mechanism, rate capacity, and cycling ability [16,27–30].

* Corresponding author.
E-mail address: 15216105346@163.com (J. Li).

http://dx.doi.org/10.1016/j.jssc.2016.05.002
0022-4596/

Motivated by this, in this work, for the first time, first-principles calculations on Na, Mg and Al base metal doping on $LiVPO_4F$ materials were performed and the effects of metal cation doping on the structure, electronic properties, defect properties and Li ions migration of pristine $LiVPO_4F$ and doped $LiVPO_4F$ materials were systematically investigated, including the following eight doping models: $Li_{0.875}Na_{0.125}VPO_4F$, $Li_{0.75}Mg_{0.125}VPO_4F$, α-$LiMg_{0.375}V_{0.75}PO_4F$, β-$LiMg_{0.375}V_{0.75}PO_4F$ and γ- $LiMg_{0.375}V_{0.75}PO_4F$, $Li_{0.725}Al_{0.125}VPO_4F$, α-$LiAl_{0.125}V_{0.875}PO_4F$ and β- $LiAl_{0.125}V_{0.875}PO_4F$.

2. Calculational methodology and models

In this work, all calculations were performed using the density functional theory (DFT) with exchange-correlation functional treated in the spin-polarized GGA-PBE [31] as implemented in the CASTEP package [32]. Ultrasoft pseudo potentials (USPP) introduced by Vanderbilt [33] have been employed for all ion-electron interactions. Convergences were tested with respect to values of energy cutoff as well as *k*-point mesh. Based on the convergence results, an energy cutoff of 500 eV was chosen in order to ensure that total energies were converged within 1×10^{-6} eV/atom. Brillouin zone sampling of the bulk material was carried out with a $3\times3\times2$ *k*-points mesh using the method of Monkhorst-Pack [34]. To take into account the strong correlation among *d* electrons of vanadium ions, the DFT+U method was adopted and a Hubbard-like correlation was added, using the reported values of U=3 eV for vanadium compounds [15,16,35].

In order to study $LiVPO_4F$ doped with low concentration metal ions and not losing the computational efficiency simultaneously, $(2\times2\times1)$ supercell models (Fig. 1) were applied for following calculations. As reported in the literatures [36,37], cation doping mechanism for olivine-structured $LiFePO_4$ is that Na, Mg, Al, Ti and Nb ion replaces the Li atom 4*a* site (Wyckoff notation). While Mn atom takes the place of Fe site, as reported by Nakamura. T et al. [38]. In a crystal cell of $LiVPO_4F$, there is only one crystallographic Li 2*i* site [14,39] and two different types of V 1*a*, 1*b* site [14,40], as depicted in Fig. 1. Therefore, only one Na-doped model of $Li_{0.875}Na_{0.125}VPO_4F$ was obtained, while the Mg-doped model of $Li_{0.75}Mg_{0.125}VPO_4F$ was prepared by one Mg atom replacing two Li atoms (one Li atom was replaced by a Mg atom, another Li atom was removed from the supercell creating a Li negative vacancy to keeping neutral charge). In addition, Mg atom may also substitute the V 1*a*, 1*b* site, so there are another three ways to substitute two V atoms by three Mg atoms in $LiVPO_4F$ $(2\times2\times1)$ supercells with a Mg interstitial compensation, such as α-$LiMg_{0.375}V_{0.75}PO_4F$, β-$LiMg_{0.375}V_{0.75}PO_4F$ and γ- $LiMg_{0.375}V_{0.75}PO_4F$. Inspired by the cation doping mechanism for olivine-structured $LiFePO_4$ and considering Al^{3+} having same charge with V^{3+} ion, Al atom may substitute Li 2*i* site or V 1*a*, 1*b* site of $LiVPO_4F$ crystal, so three configurations such as $Li_{0.725}Al_{0.125}VPO_4F$ (one Li atom was replaced by an Al atom and another two Li atoms were removed from the supercell creating two Li negative vacancies), α-$LiAl_{0.125}V_{0.875}PO_4F$ and β-$LiAl_{0.125}V_{0.875}PO_4F$ were obtained. For transition metal V, the property of magnetic ground state was also researched by considering ferromagnetic and antiferromagnetic structures. In the ferromagnetic structure, two types V atom were set to the same spin sequences of spin-up (high spin state, +2), while adverse spin sequences of spin-up (high spin state, +2) and spin-down (low spin state, −2) were set for antiferromagnetic structure. To determine the most-stable configuration for following calculations of electronic properties, defect properties and Li ions migration, full optimizations of the fractional coordinates and lattice parameters were performed for above eight doped models by means of total energy minimization.

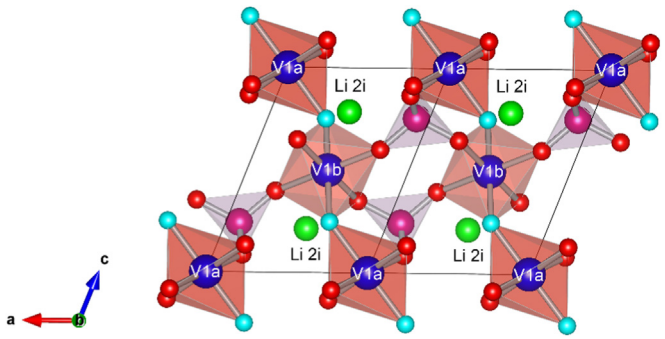

Fig. 1. Schematic representation for crystal structure and Li, V site of $2\times2\times1$ $LiVPO_4F$ supercell. Li atom in green; V atom in cyan; P atom in purple; O atom in red and F atom in blue. (For interpretation of the references to color in this figure legend, the reader is referred to the web version of this article.)

Formation energies measuring the stability of doped $LiVPO_4F$ were calculated according to the following equation: $E_f=[E(LiVPO_4F_{doped})+aE(Li)+bE(V)-E(LiVPO_4F)-cE(Metal_{dop})]$, where $E(LiVPO_4F_{doped})$, $E(LiVPO_4F)$, $E(Li)$, $E(V)$ and $E(Metal_{dop})$ is the total energy of optimized crystal unit of doped-$LiVPO_4F$, pristine $LiVPO_4F$ and the energy of a single Li, V and doping metal atom (Na, Mg and Al), respectively. Here, entropy, volume change, and temperature effects were all ignored. In addition, the transition-state searches for Li ions migration paths and activation barriers were probed by the LST/QST method [41] as implemented in the CASTEP package.

3. Results and discussion

3.1. Crystal structure and formation energy

Crystal structure of $LiVPO_4F$ belongs to the triclinic space group $P\bar{1}$ [14], as depicted in Fig. 1. In a $LiVPO_4F$ cell, lithium ions reside within the interstitial spaces to form Li 2*i* sites. $LiVPO_4F$ crystallizes into a mineral tavorite-like structure that comprises a three-dimensional network built up those chains of distorted VO_4F_2 octahedra sharing two fluorine atoms, where neighboring chains were connected by the O atom corner-sharing PO_4 tetrahedra [40]. The results of energy calculations show that energy of ferromagnetic phase is slightly lower by 10 meV compared to the antiferromagnetic structure. Therefore, ferromagnetic phase represents the magnetic ground state, and for all following calculations of pristine and doped $LiVPO_4F$, only ferromagnetic phase was considered.

The calculated and experimental formation energies, lattice constants and volumes of $2\times2\times1$ $LiVPO_4F$ supercell are listed in Table 1. It is can be seen that the calculated lattice constants for $LiVPO_4F$ are slightly smaller than corresponding experimental values with a discrepancy of 1.8% [14], it is due to the fact that GGA usually overestimate the lattice constants for a system. However, our slights mainly focus on the effect of Na, Mg and Al on the structure, electronic properties and ionic conductivity of doping $LiVPO_4F$ materials, so the relative values of calculated results should be paid great attention to, rather than the absolute values.

The process of substituting one Li atom with Na to form $Li_{0.875}Na_{0.125}VPO_4F$ is slightly exothermic (−0.015 eV, −1.44 KJ/mol), which indicates this process is spontaneous. Therefore, Na doping at Li 2*i* site in $LiVPO_4F$ to form $Li_{0.875}Na_{0.125}VPO_4F$ structure is reasonable and exercisable. Seen from Table 1, $Li_{0.875}Na_{0.125}VPO_4F$ has the triclinic structure, with the lattice constants of $a=10.43$ Å, $b=10.72$ Å and $c=7.37$ Å. Compared to pristine $LiVPO_4F$, the volume of $Li_{0.875}Na_{0.125}VPO_4F$ structure increases by 0.14%, indicating that Na doping does not significantly affect the structure of $LiVPO_4F$ and still keep stability of doped-$LiVPO_4F$. Moreover, the lattice stabilization is

also provided by the orthophosphate anion (PO_4^{3-}) matrix, which has relatively strong P-O bonds [42].

For $Li_{0.75}Mg_{0.125}VPO_4F$, the formation energy of an Mg atom substituting two Li sites is positive (4.897 eV, 470.11 KJ/mol), which means even higher temperature far above 0 K cannot proceed this substitution process. In addition, formation energy of γ-$LiMg_{0.375}V_{0.75}PO_4F$ is also positive (6.24 eV, 599 KJ/mol), in which three Mg atoms simultaneously replace the V1*a* and V1*b* sites and generate an Mg interstitial atom. Therefore, the $Li_{0.75}Mg_{0.125}VPO_4F$ and γ-$LiMg_{0.375}V_{0.75}PO_4F$ models were abandoned in the following discussions of electronic properties and Li ions diffusion. However, formation energy of α-$LiMg_{0.375}V_{0.75}PO_4F$ and β-$LiMg_{0.375}V_{0.75}PO_4F$ is −0.229 and −0.123 eV, respectively. Due to an extra Mg being inserted into the interstitial site to maintain charge balance, the volume of α-$LiMg_{0.375}V_{0.75}PO_4F$ and β-$LiMg_{0.375}V_{0.75}PO_4F$ all expand slightly by 1.19% and 0.25%, respectively.

Similar to $Li_{0.75}Mg_{0.125}VPO_4F$, the process of an Al atom replacing three Li atoms to form $Li_{5/8}Al_{1/8}VPO_4F$ is thermodynamic prohibited. Corresponding formation energy is 7.636 eV (733 KJ/mol). While for α-$LiAl_{0.125}V_{0.875}PO_4F$ and β-$LiAl_{0.125}V_{0.875}PO_4F$, the formation energy of them are all negative, as −1.148 and −1.29 eV, respectively. This indicates that Al atoms occupying the V sites to replace a part of V atoms is thermodynamically stable and feasible. After Al atoms being introduced, the volume of α-$LiAl_{0.125}V_{0.875}PO_4F$ and β-$LiAl_{0.125}V_{0.875}PO_4F$ shrink by −1.37% and 1.34%, respectively, it is due to the smaller Al atom than V. Moreover, Al doping does not obviously change the structure and still keep structural stability of Al doped-$LiVPO_4F$. Therefore, only α-$LiAl_{0.125}V_{0.875}PO_4F$ and β-$LiAl_{0.125}V_{0.875}PO_4F$ were discussed about electronic properties and Li ions diffusion.

3.2. Electronic properties of doped $LiVPO_4F$

3.2.1. Pristine $LiVPO_4F$

To clarify the effect of Na, Mg and Al on the electronic properties of $LiVPO_4F$ material, energy band structures along the high symmetry point across the first Brillouin zone and spin polarized electron density of states (DOS) of pristine ferromagnetic phase $LiVPO_4F$ were calculated. The corresponding results were presented in Figs. 2(a) and 3(a). Viewed from Fig. 2(a) that $LiVPO_4F$ behaves as a semiconductor with an indirect gap of 1.635 eV. This value is in good agreement with the previous work of 1.63 eV [43], but it should be certain that this calculated result of 1.635 eV is less than the experimental value. Here, only the relative differences of doped and pristine $LiVPO_4F$ need to cared, so the disadvantages of GGA underestimating gaps can be ignored.

In this work, the partial electron density of states (PDOS) only showed electron state distributing between −10 to 10 eV and leave out the parts of lower energy due to them not taking part in forming bond process. It can be seen that the top of valence band and bottom of conduction band were mainly occupied by V-3*d* spin up orbital as well as hybridization with O-2*p* and F-2*p* spin up orbitals, which means good performances of electron transport in the charge and discharge process. In addition, the total DOS of spin up and spin down above −1 eV are inconsistent, a total of 2 μ_B per $LiVPO_4F$ unit, which is just the reflection of ferromagnetic phase structure.

3.2.2. Na doped $LiVPO_4F$

Usually, electrical conductivity of a system is determined by the electronic structure property, so in the following discussion energy

Table 1
Calculated and experimental formation energies, lattice constants, volumes and band gaps of (2 × 2 × 1) $LiVPO_4F$ supercell.

	Formation energy (eV)	Lattice constants/Å			Angle/°			V (Å^3)	ΔV/V%	Band gap (eV)
		a	*b*	*c*	α	β	γ			
$LiVPO_4F$(Exp)		10.34	10.61	7.26	72.41	107.97	81.61	697.44		
$LiVPO_4F$		10.39	10.69	7.39	71.48	107.68	82.78	718.78		1.635
$Li_{0.875}Na_{0.125}VPO_4F$	−0.015	10.43	10.72	7.37	71.46	107.29	81.66	719.78	0.14	1.437
$Li_{0.75}Mg_{0.125}VPO_4F$	4.897	10.45	10.67	7.41	70.78	107.39	83.19	723.01	0.59	
α-$LiMg_{0.375}V_{0.75}PO_4F$	−0.229	10.47	10.68	7.44	71.07	107.85	83.47	727.36	1.19	1.376
β-$LiMg_{0.375}V_{0.75}PO_4F$	−0.123	10.33	10.78	7.42	70.68	107.00	82.08	720.56	0.25	1.341
γ-$LiMg_{0.375}V_{0.75}PO_4F$	6.24	10.42	10.77	7.44	71.01	107.64	83.3	730.85	1.68	
$Li_{5/8}Al_{1/8}VPO_4F$	7.636	10.40	10.66	7.41	70.65	107.48	83.81	719.66	0.12	
α-$LiAl_{0.125}V_{0.875}PO_4F$	−1.148	10.37	10.62	7.36	71.66	107.77	82.47	708.92	−1.37	1.400
β-$LiAl_{0.125}V_{0.875}PO_4F$	−1.290	10.34	10.67	7.35	71.41	107.71	82.62	709.14	−1.34	1.419

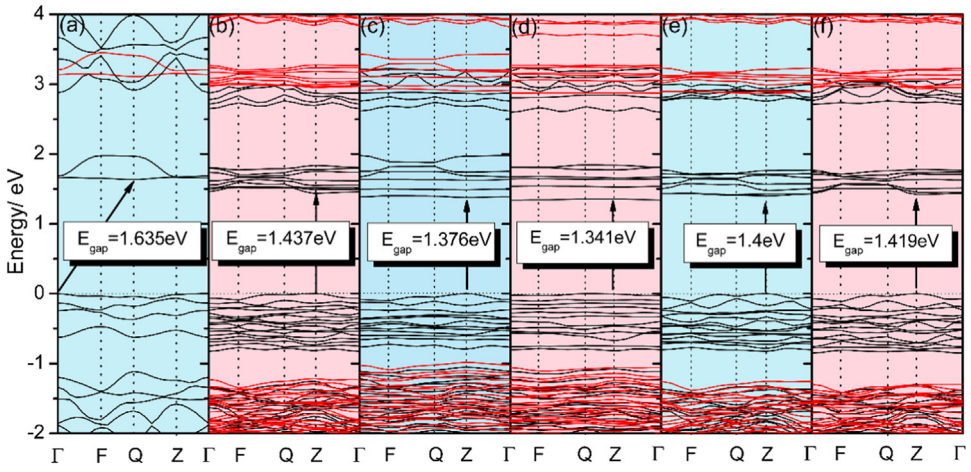

Fig. 2. Calculated band structure along the high symmetry point of (a) pristine $LiVPO_4F$, (b) $Li_{0.875}Na_{0.125}VPO_4F$, (c) α-$LiMg_{0.375}V_{0.75}PO_4F$, (d) β-$LiMg_{0.375}V_{0.75}PO_4F$, (e) α-$LiAl_{0.125}V_{0.875}PO_4F$ and (f) β-$LiAl_{0.125}V_{0.875}PO_4F$.

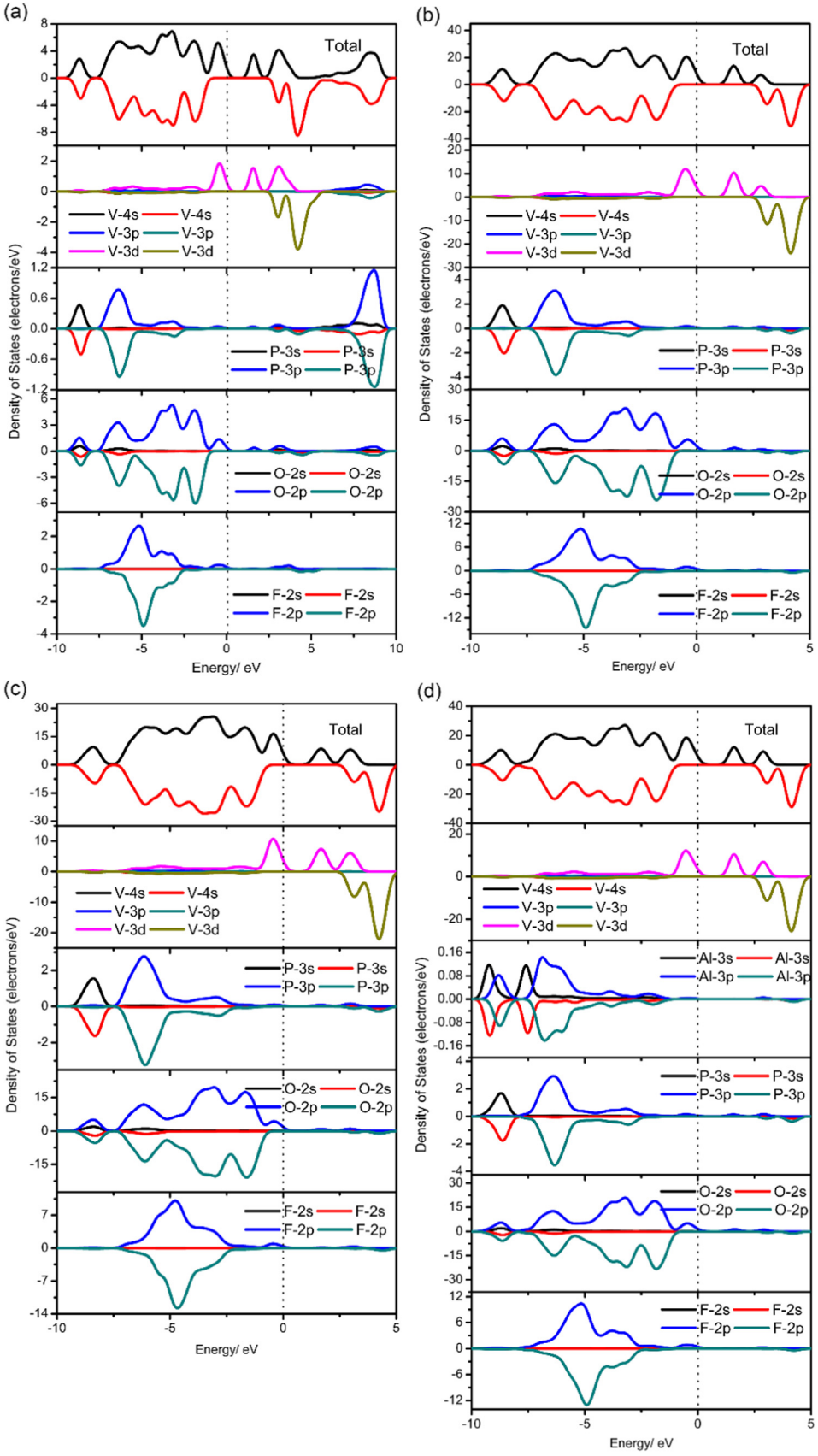

Fig. 3. Electron density of states (DOS) and partial electron density of states (PDOS) of (a) pristine $LiVPO_4F$ (around the Fermi level); (b) $Li_{0.875}Na_{0.125}VPO_4F$; (c) α-$LiMg_{0.375}V_{0.75}PO_4F$; (d) α-$LiAl_{0.125}V_{0.875}PO_4F$.

band structure and density of state were mainly focused on [44]. Fig. 2(b) shows calculated energy band structure of $Li_{0.875}Na_{0.125}VPO_4F$. Observed from Fig. 2(b), Na-doping gives rise to the decrease of conduction band, therefore leading to a reduction of band gap from 1.635 ($LiVPO_4F$) to 1.437 eV ($Li_{0.875}Na_{0.125}VPO_4F$). In addition, band gap of Na doped $LiVPO_4F$ changes from an indirect gap of pristine $LiVPO_4F$ to a direct gap. All these results indicate that replacing a few of Li atoms with Na is able to improve the electrical conductivity of $LiVPO_4F$ system.

To clearly insight the details near the Fermi level, spin polarized partial density of states (PDOS) between −10 to 5 eV were depicted in Fig. 3(b). Unlike pristine $LiVPO_4F$, the upper conduction bands of $Li_{0.875}Na_{0.125}VPO_4F$ are no longer dominated by V-3*p*, P-3*p* and O-2*p* orbitals, so the width of conduction bands of $Li_{0.875}Na_{0.125}VPO_4F$ system is 5 eV, less than that 10 eV of pristine $LiVPO_4F$. Like the case of undoped-$LiVPO_4F$, the total DOS of $Li_{0.875}Na_{0.125}VPO_4F$ near the Fermi level depends on its PDOS of V-3*d* spin up orbital as well as hybridization with O-2*p* and F-2*p* spin up orbitals. In addition, PDOS of Na is not depicted due to no electron state around the Fermi level. In other words, the doped Na atoms cannot change band gap directly, and the band gap shrink of $Li_{0.875}Na_{0.125}VPO_4F$ is due to the change of electronic structures of V-3*d* spin up orbitals.

According to the crystal-field theory, the 3*d* orbital of V ion in the octahedral center is split into lower energy $t_{2\,g}$ orbital (d_{xy}, d_{xz} and d_{yz}) and higher energy e_g orbital ($d_{x^2-y^2}$ and d_{z^2}) [45,46], as depicted in Fig. 4. As a larger Na atom is introduced to the Li 2*i* site, on one hand, it expands the lattice volume, resulting in the distortion of V octahedron [47]. On the other hand, Na atom substituting Li slightly reduces the charge of its surrounding O atoms (see Fig. 5, decrease by 0.02 *e*), so the weakened electrostatic fields of O atoms partly ease the split of e_g orbital and t_{2g} orbital of central atom V-3*d* (see Fig. 4). Therefore, the second peak in conduction band (about 3 eV) of V-3*d* spin up PDOS weaken, and the bottom of conduction band shifts to low energy (Fig. 3(a)). It is noteworthy that this mechanism for enhancing electrical conductivity of Na-doped $LiVPO_4F$ is slightly different from those transition metals doping with 3*d* electrons for olivine-structured $LiFePO_4$ [37,48].

3.2.3. Mg-doped $LiVPO_4F$

The calculated results of energy band structure and spin polarized total density of states (DOS) of Mg-doped $LiVPO_4F$ were demonstrated in Figs. 2(c), d and 3(c). Compared to $LiVPO_4F$ in Fig. 2(a), the direct band gap of α-$LiMg_{0.375}V_{0.75}PO_4F$ and β-$LiMg_{0.375}V_{0.75}PO_4F$ was narrowed down to 1.376 and 1.341 eV, respectively, due to the decrease of corresponding conduction band bottom. It indicates that the electrical conductivity performance of $LiVPO_4F$ can be significantly lifted by bits of replacements of V atoms with Mg. Seen from Fig. 3(c), the electronic state near the Fermi level is absolutely dominated by the V-3*d* spin up orbital as well as hybridization with its neighboring O-2*p* and F-2*p*, which is similar to Na-doped $LiVPO_4F$. In Fig. 3(c), PDOS of Mg atom are not illustrated because of no electronic state distributing near the Fermi level. These evidences demonstrate that the introduced Mg atoms at V sites also indirectly reduce band gaps of α-$LiMg_{0.375}V_{0.75}PO_4F$ and β-$LiMg_{0.375}V_{0.75}PO_4F$, through changing the electronic structures of V-3*d* spin up orbital. Specifically, the two Mg atoms and an interstitial Mg give rise to the lattice expansion of Mg-doped $LiVPO_4F$. Accordingly the distortion of V octahedron and the ease of 3*d* split orbitals shift the bottom of conduction band to low energy and reduces band gaps of α-$LiMg_{0.375}V_{0.75}PO_4F$ and β-$LiMg_{0.375}V_{0.75}PO_4F$.

3.2.4. Al-doped $LiVPO_4F$

Figs. 2(e), f and 3(d) show calculated energy band structure and spin polarized partial density of states (PDOS) of Al-doped $LiVPO_4F$, as α-$LiAl_{0.125}V_{0.875}PO_4F$ and β-$LiAl_{0.125}V_{0.875}PO_4F$. Compared to pristine $LiVPO_4F$, the conduction band for α-$LiAl_{0.125}V_{0.875}PO_4F$ and β-$LiAl_{0.125}V_{0.875}PO_4F$ decreases by −0.235 and −0.216 eV, respectively, which gives rise to a narrower band gap of 1.4 and 1.419 eV. The smaller band gaps demonstrate that a trace of replacement of V atoms with Al can crucially enhance the electrical conductivity of $LiVPO_4F$, and it is consistent with the previous experimental report that Al doping can improve ionic or electronic transmission [23]. To further insight the influences of Al-doping on the electronic properties of $LiVPO_4F$ around the Fermi level, PDOS of V atom were also depicted in Fig. 3(d). The calculated results reveal that DOS at the Fermi level is absolutely dominated by V-3*d* spin up orbital, which hybrids with its neighboring orbitals of O-2*p* and F-2*p*.

The mechanism of Al-doping enhancing the electrical conductivity of $LiVPO_4F$ is similar to Na and Mg-doping, because of similar total DOS curve around Fermi level for both Na, Mg and Al-doped $LiVPO_4F$ (Fig. 3(b), c and d) in the sense. The introduced Al atoms at V sites also indirectly reduce band gaps of α-$LiAl_{0.125}V_{0.875}PO_4F$ and β-$LiAl_{0.125}V_{0.875}PO_4F$, through changing the electronic structures of V-3*d* spin up orbital. Similarly, the weakening of second peak of PDOS (V-3*d* spin up, area of high energy) caused by the distortion of V octahedron and the ease of 3*d* split orbitals shifts the bottom of conduction band to low

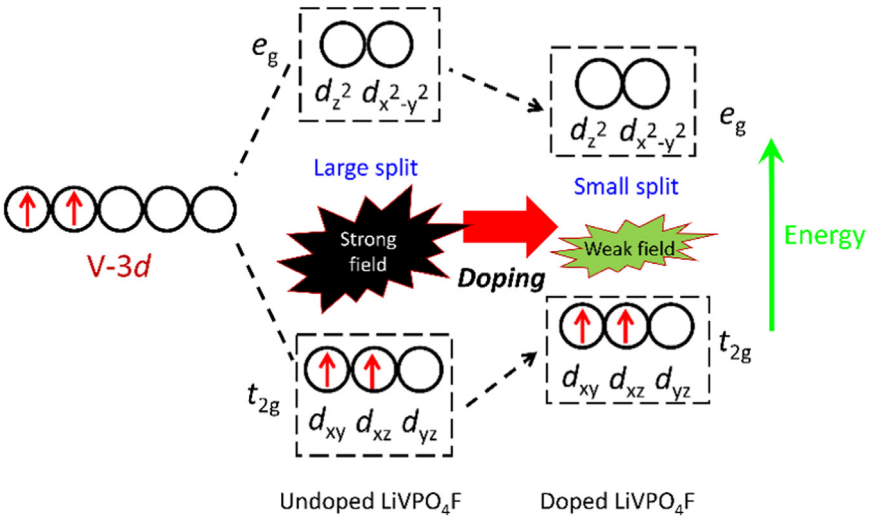

Fig. 4. Split 3*d* orbital energy level diagram of V^{3+} in $LiVPO_4F$ and doped $LiVPO_4F$.

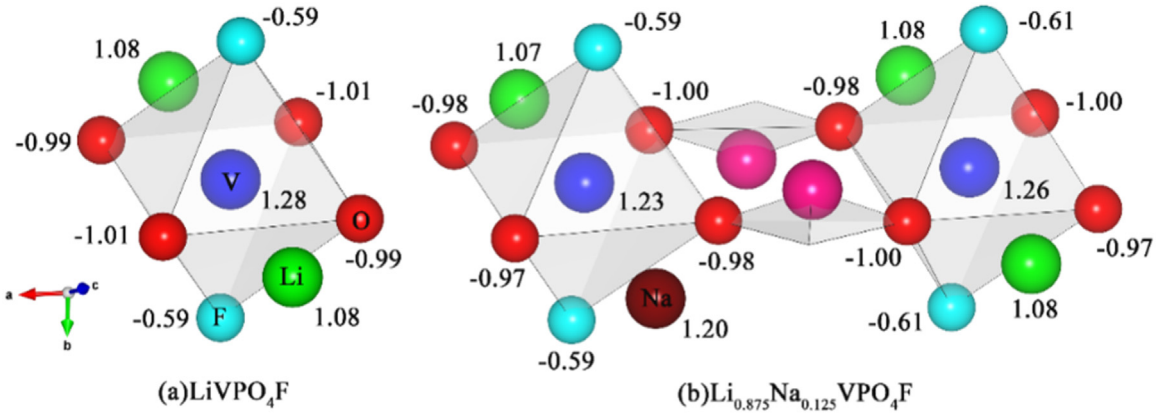

Fig. 5. Mulliken charge of the V octahedron in (a) $LiVPO_4F$ and (b) $Li_{0.875}Na_{0.125}VPO_4F$ (unit: e).

energy and reduces the band gap of α-$LiAl_{0.125}V_{0.875}PO_4F$ and β-$LiAl_{0.125}V_{0.875}PO_4F$ accordingly.

From above analysis of band gaps (listed in Table 1) and DOS, Na, Mg and Al metal doping can significantly improve electrical conductivity of $LiVPO_4F$ material and simultaneously maintain structural stability. Hereto, the same doping mechanism of the change of V-3*d* spin up orbital arisen from the distortions of V octahedron by lattice changes has been discovered. Moreover, the influence of V site doping by Mg and Al on electrical conductivity of $LiVPO_4F$ material is obviously better than Na doping at the Li site.

3.3. Intrinsic defect properties of pristine $LiVPO_4F$

To fully understand the electrochemical properties and Li ion diffusion behaviors of cathode materials, knowledge of the intrinsic point defect and associated properties is crucial. Given these isolated point defects (vacancy and interstitial) are the intrinsic characteristics of lattice vibrations [49]. In this section, two types of defects, such as Li, V, P, O and F atom Schottky defect and only Li Frenkel defects have been discussed due to its smaller ionic radius for interstitial. To prepare starting structure for defective system, full optimizations for atomic fractional coordinates of nondefective supercell were firstly carried out. In order to simulate low concentration Schottky vacancy defect, one atom was removed from $(2\times2\times1)$ supercells. Subsequently, these defective models were fully optimized without symmetry constraints. The formation energy of one atom Schottky vacancy defect E_{De}[S] is defined as the following equation: $E_{De}[S]= E_S [S]+ E[atom]–E_S$, here, E_S [S] and E_S is the total energy of optimized supercell structure with and without one atom vacancy, respectively, and E [atom] is the point energy of one atom in a cubic box. The calculated Schottky defect formation energy of pristine $LiVPO_4F$ for Li, V1*a*, V1*b*, P, O and F atom were all listed in Table 2. These Schottky defect formation energies are all positive, implying that forming a vacancy defect needs to absorb energy and Li vacancy defect is favorable with the lowest formation energy of 0.55 eV. In particular, central atoms vanadium and phosphorus vacancies are highly unfavorable and thus unlikely to occur in any significant concentration in $LiVPO_4F$ material.

Table 2
Calculated formation energy (in eV) for one atom Schottky defect E_{De}[S] and Frenkel defect E_{De}[Fr] of pristine $LiVPO_4F$.

Point defect	Li	V1a	V1b	P	O	F
E_{De}[S]	0.55	10.58	9.42	10.33	3.50	1.48
E_{De}[Fr]	7.35					

A Frenkel defect is a vacancy-interstitial pair formed when an atom jumps from a normal lattice point to an interstitial site. To establish cation Frenkel defects, a Li atom was undocked from its original position to form a vacancy site and was placed at interstitial sites for pristine $LiVPO_4F$. The formation energy of Li Frenkel defect E_{De}[Fr] was calculated according to the following equation: $E_{De}[Fr] = E_F[Fr]-E_F$, where E_F[Fr] and E_F is the total energy of the optimized supercell structure with and without Li atom Frenkel defect, respectively. The calculated result of Li Frenkel defect formation energy was also summarized in Table 2. It is can be seen that Li atom Frenkel formation energy (7.35 eV) of $LiVPO_4F$ is much significantly larger than its corresponding Schottky defect (0.55 eV).

All these evidences reveal that Li atom vacancy defects in real $LiVPO_4F$ are not ignorable at room temperature, and vacancy defects with a lower activation energy for Li atom is far more likely to occur than corresponding Frenkel defects. Moreover, it is worth noting that the concentration of point defects is also sensitive to synthesis conditions and thermal history.

3.4. Li ions migration in pristine and doped $LiVPO_4F$

Apart from electrical conductivity, intrinsic ionic conductivity of $LiVPO_4F$ also has a significant importance on the electrochemical performance [16,50]. In the electrode system of Li-ion batteries, Li ion is the only carrier of ionic transport. Although total diffusion coefficient can be measured by experiments, it is generally difficult to figure out the microscopic diffusion mechanism [11]. Fortunately, theoretical calculations can provide probability for figuring out the migration energy barriers and elucidating diffusion pathways and their dimensionality. In $LiVPO_4F$ unit cell, there is only one Li site (labeled as Li-2*i* in Fig. 1(a)). Based on it, four main possible linear diffusion paths between adjacent Li sites were considered, as shown in Fig. 6. Path A is along the *a* axis [100] direction with a jump distance of about 5.194 Å, path B is along the *b* axis of [010] direction with a jump distance of about 5.348 Å, path C is along the [0.488 0.17 0. $\bar{5}$72] direction with a jump distance of about 7.568 Å and path D is along the [0.012 0.$\bar{1}$7 0.572] direction with the shortest jump distance of about 3.987 Å.

In this work, only the favorable vacancy hopping mechanism for Li ion intrinsic migration was considered due to the fact that it is more energetically favorable than that diffusing through an interstitial site mechanism, as demonstrated in Section 3.3. One lithium ion was extracted from one $(2\times2\times1)$ $LiVPO_4F$ supercell to generate a lithium vacancy as the initial configuration, while the final configuration was created by extracting one lithium atom in the specified directions from another $(2\times2\times1)$ $LiVPO_4F$ supercell, where this lithium vacancy was adjacent to that in the initial configuration (Fig. 6). When lithium was diffusing, positions of the

other atoms remain unchanged. The energy barriers were obtained through monitoring the position of highest potential energy along the migration path [11].

Fig. 7(a) and Table 3 show calculated energy curves and activation energies of Li ion diffusion via vacancy hopping mechanism along four specified directions in pristine $LiVPO_4F$ $(2\times2\times1)$ supercell. There are two key points from the calculated results. On one hand, for pristine $LiVPO_4F$, path D along the [0.012 0.$\bar{1}$7 0.572] direction is found to have a lowest activation energy (0.418 eV) with a hopping distance of about 3.987 Å. On the other hand, Li ion immigrates in other paths, the corresponding activation energies are all found to have prohibitively high values (>2.0 eV). All these results are more than 5 orders of magnitude higher than path D along the [0.012 0.$\bar{1}$7 0.572] direction, suggesting that the anisotropic nature of Li ion conduction in this material and $LiVPO_4F$ is a one-dimensional (1D)-ion conductor. In addition, the calculated activation energy of 0.418 eV for lithium migration through mineral tavorite $LiVPO_4F$ materials sustains experimental facts that these materials have relatively better performance of lithium diffusion. Our calculated values of 0.418 eV is consistent with experimental activation energies for Li diffusion in other related cathodes or LISICON-type materials [51]. For convenient comparison with the experimental results of Li ion diffusion coefficients in $LiVPO_4F/VPO_4F$ system, this diffusion coefficient was derived by according migration activation energy.

According to the dilute diffusion theory, diffusion coefficient of any ion or vacancy hopping can be predicted by using the following formula [52]: $D=g\Gamma a^2$, here, D is the diffusion coefficient, g is the geometric factor, and a is the corresponding ionic jump distance of about 3.987 Å. In addition, Γ is the jumping frequency, defined based on the transition-state theory [53]: $\Gamma=\nu\ \exp(-E_a/kT)$. Where, ν is the attempt frequency and E_a is the migration activation energy. Therefore, activation energy offers a direct estimate about the diffusion coefficient for an assumed jump distance. In this work, g is set as 1 and ν is equal to the typical value of 10^{13} Hz [53]. For the favorable activation energies in $LiVPO_4F$, diffusion coefficient was estimated to be 2.82×10^{-9} cm^2/s (273 K) in the [0.012 0.$\bar{1}$7 0.572] direction, which reveals a good agreement with the calculated result of 2×10^{-9} cm^2/s by Tim Mueller et al. [54] and the corresponding experimental values. Depending upon synthesis conditions, experimental values of Li^+ diffusion coefficient in fluorophosphate tavorites $LiVPO_4F/VPO_4F$ system measured by GITT, EIS and CV techniques were reported as following: 10^{-15}–10^{-9} cm^2/s [55], 10^{-14}–10^{-8} cm^2/s [56].

In order to study the influence of Na, Mg and Al doping on Li ion diffusion activation energy, the energy calculations of Li ion diffusion along the [0.012 0.$\bar{1}$7 0.572] direction via favorable vacancy hopping mechanism in doped $LiVPO_4F$ were performed. The calculated energy curves and activation energies are depicted in Fig. 7(b) and Table 3, at the first glance, Na, Mg and Al doping all go against Li mobility to varying degrees. Mg and Al doping significantly increases the activation energies of Li diffusion compared to pristine $LiVPO_4F$. For Mg-doped $LiVPO_4F$, the introduced interstitial Mg atoms not only change its surrounding environment, but the strong repulsive interaction between Mg and Li also hinder Li ions from migrating to the adjacent Li sites. Different from Mg-doped $LiVPO_4F$, the activation energies (0.69 and

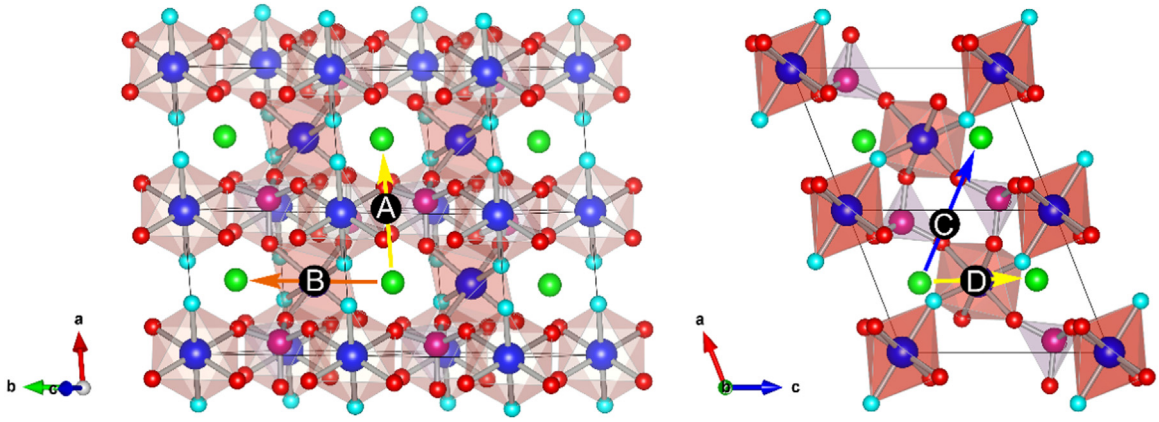

Fig. 6. Li diffusion via vacancy mechanism for a Li ion jump from an initial site to the first nearest vacancy location.

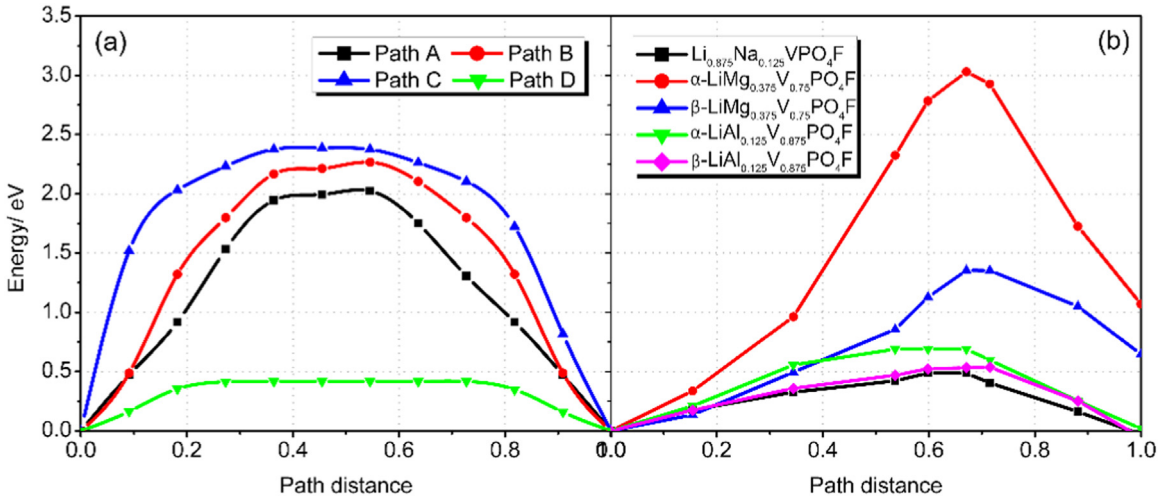

Fig. 7. Energy profile for the Li ion hoping via vacancy mechanism between four specified paths in (a) pristine $LiVPO_4F$ and (b) Li ion hoping by path D in five doped $LiVPO_4F$.

Table 3
Calculated activation energy (in eV) for Li ion hoping in pristine and doped $LiVPO_4F$.

	Path direction	Activation energy
$LiVPO_4F$	A-[100]	2.025
	B-[010]	2.267
	C-[0.488 0.17 0. $\bar{5}$72]	2.387
	D-[0.012 0.$\bar{1}$7 0.572]	0.418
$Li_{0.875}Na_{0.125}VPO_4F$	D-[0.012 0.$\bar{1}$7 0.572]	0.487
α-$LiMg_{0.375}V_{0.75}PO_4F$	D-[0.012 0.$\bar{1}$7 0.572]	3.03
β-$LiMg_{0.375}V_{0.75}PO_4F$	D-[0.012 0.$\bar{1}$7 0.572]	1.354
α-$LiAl_{0.125}V_{0.875}PO_4F$	D-[0.012 0.$\bar{1}$7 0.572]	0.69
β-$LiAl_{0.125}V_{0.875}PO_4F$	D-[0.012 0.$\bar{1}$7 0.572]	0.535

0.535 eV) of Li diffusion in Al-doped $LiVPO_4F$ are slightly larger than that in pristine, as evidence in Table 1, Al doping can shrink all the lattice constants *a*, *b* and *c*, so the diffusion channels along the [0.012 0.$\bar{1}$7 0.572] direction narrow down. All these disadvantages lead to a minor increase of activation energies for Li ions diffusion in doped $LiVPO_4F$. Among all these metal doping, the activation energy (0.487 eV) of Na doped $LiVPO_4F$ is more close to that 0.418 eV of pristine $LiVPO_4F$, indicating Na doping has a negligible side effect on the Li ion mobility.

Combined with the experimental facts of Na and Al doping making better electrochemical behaviors such as cyclic performance and rate capability [23,25], a conclusion was drawn that Na, Mg and Al doping can significantly improve some electrochemical behaviors of $LiVPO_4F$ material by enhancing its electrical conductivity, although some side effects on Li migration.

4. Conclusion

The effects of Na, Mg and Al base metal doping on the structure, electronic properties, defect properties and Li ions migration of $LiVPO_4F$ and doped $LiVPO_4F$ materials were studied by the first-principles method based on the density functional theory (DFT). The following conclusions are drawn based on the calculations:

a) These synthesis processes of Na doping in the Li sites to form $Li_{0.875}Na_{0.125}VPO_4F$, Mg replacing the V sites to form α-$LiMg_{0.375}V_{0.75}PO_4F$ and β-$LiMg_{0.375}V_{0.75}PO_4F$, Al substituting the V sites to form α-$LiAl_{0.125}V_{0.875}PO_4F$ and β-$LiAl_{0.125}V_{0.875}PO_4F$ are all feasible.
b) Na, Mg and Al metal doping can significantly improve the electrical conductivity of $LiVPO_4F$ material and simultaneously maintain the structural stability. Good performance of electrical conductivity attributing to the reduction of band gaps through changing the electronic structures of V-3*d* spin up orbital arisen from the distortions of V octahedron by lattice changes and the ease of 3*d* split orbitals. Moreover, the influence of V site doping by Mg and Al on electrical conductivity of $LiVPO_4F$ material is obviously better than the case of Na doping at the Li site.
c) Li vacancy defects in $LiVPO_4F$ are not ignorable at room temperature, and these vacancy defects with a lower activation energy for Li atom are far more likely to occur than Frenkel defects for Li and vacancy defects for other atoms.
d) For the pristine $LiVPO_4F$, path D along the [0.012 0.$\bar{1}$7 0.572] direction is found to have the lowest activation energy of 0.418 eV, suggesting that the anisotropic nature of Li ion conduction in this material and $LiVPO_4F$ is a one-dimensional (1D)-ion conductor. The corresponding diffusion coefficient was estimated to be 2.82×10^{-9} cm^2/s, which is in good agreement with the experimental values.
e) Combined with the experimental facts, Na, Mg and Al doping can significantly improve some electrochemical behaviors of $LiVPO_4F$ material by enhancing its electrical conductivity, although these doping all go against Li mobility to varying degrees.

Acknowledgements

We sincerely acknowledge the High Performance Computing Center of CSU, China. This work was financially supported by the National Science and Technology Support Project of China (No. 2012BAE08B02) and National Natural Science Foundation of China (No. 51264011).

Appendix A. Supporting information

Supplementary data associated with this article can be found in the online version at http://dx.doi.org/10.1016/j.jssc.2016.05.002.

References

[1] Y. Chen, S. Sun, X. Wang, Q. Shi, Study of lithium migration pathways in the organic electrode materials of li-battery by dispersion-corrected density functional theory, J. Phys. Chem. C 119 (2015) 25719–25725.
[2] E. Castel, E.J. Berg, M. El Kazzi, P. Novák, C. Villevieille, Differential electrochemical mass spectrometry study of the interface of $xLi_2MnO_3 \cdot (1–x)LiMO_2$ (M=Ni, Co, and Mn) material as a positive electrode in Li-ion batteries, Chem. Mater. 26 (2014) 5051–5057.
[3] N. Lespes, J.S. Filhol, Using implicit solvent in Ab initio electrochemical modeling: investigating Li(+)/Li electrochemistry at a Li/solvent interface, J. Chem. Theory Comput. 11 (2015) 3375–3382.
[4] D. Mikhailova, A. Sarapulova, A. Voss, A. Thomas, S. Oswald, W. Gruner, D. M. Trots, N.N. Bramnik, H. Ehrenberg, $Li_3V(MoO_4)_3$: a new material for both Li extraction and insertion, Chem. Mater. 22 (2010) 3165–3173.
[5] Z. Xu, X. Lv, J. Li, J. Chen, Q. Liu, A promising anode material for sodium-ion battery with high capacity and high diffusion ability: graphyne and graphdiyne, RSC Adv. 6 (2016) 25594–25600.
[6] Y. Koyama, I. Tanaka, M. Nagao, R. Kanno, First-principles study on lithium removal from Li_2MnO_3, J. Power Sources 189 (2009) 798–801.
[7] S.H. Chen, Z.R. Xiao, P.H. Lee, Y.P. Liu, Y.K. Wang, Stability of half-metallic antiferromagnet La_2VMnO_6, first-principles calculation study, Physica B: Condens. Matter 406 (2011) 2783–2787.
[8] P. Yan, L. Xiao, J. Zheng, Y. Zhou, Y. He, X. Zu, S.X. Mao, J. Xiao, F. Gao, J.-G. Zhang, C.-M. Wang, Probing the degradation mechanism of Li_2MnO_3 cathode for Li-ion batteries, Chem. Mater. 27 (2015) 975–982.
[9] Y. Lyu, N. Zhao, E. Hu, R. Xiao, X. Yu, L. Gu, X.-Q. Yang, H. Li, Probing reversible multielectron transfer and structure evolution of $Li_{1.2}Cr_{0.4}Mn_{0.4}O_2$ cathode material for Li-ion batteries in a voltage range of 1.0–4.8 V, Chem. Mater. 27 (2015) 5238–5252.
[10] M. Sumita, Y. Tanaka, M. Ikeda, T. Ohno, Theoretically designed $Li_3PO_4(100)/LiFePO_4(010)$ coherent electrolyte/cathode interface for all solid-state Li Ion secondary batteries, J. Phys. Chem. C 119 (2015) 14–22.
[11] C. Ouyang, S. Shi, Z. Wang, X. Huang, L. Chen, First-principles study of Li ion diffusion in $LiFePO_4$, Phys. Rev. B 69 (2004) 104303.
[12] S. Shi, C. Ouyang, Z. Xiong, L. Liu, Z. Wang, H. Li, D.-s. Wang, L. Chen, X. Huang, First-principles investigation of the structural, magnetic, and electronic properties of olivine $LiFePO_4$, Phys. Rev. B 71 (2005) 144404.
[13] T. Maxisch, G. Ceder, Elastic properties of olivine Li_xFePO_4 from first principles, Phys. Rev. B 73 (2006) 174112.
[14] J.M. Ateba Mba, C. Masquelier, E. Suard, L. Croguennec, Synthesis and crystallographic study of homeotypic $LiVPO_4F$ and $LiVPO_4O$, Chem. Mater. 24 (2012) 1223–1234.
[15] Y. Li, B. Huang, X. Cheng, Y. Zhang, Achieving high specific capacity through a two-electron reaction in hypothetical Li_2VFSiO_4: a first-principles investigation, J. Electrochem. Soc. 162 (2015) A787–A792.
[16] M.M. Islam, M. Wilkening, P. Heitjans, T. Bredow, Insights into Li(+) migration pathways in alpha-$Li3_VF_6$: a first-principles investigation, J. Phys. Chem. Lett. 3 (2012) 3120–3124.
[17] J. Barker, M.Y. Saidi, J.L. Swoyer, A comparative investigation of the Li insertion properties of the novel fluorophosphate phases, NaVPO[sub 4]F and LiVPO[sub 4]F, J. Electrochem. Soc. 151 (2004) A1670.
[18] J. Barker, M.Y. Saidi, J.L. Swoyer, Electrochemical insertion properties of the novel lithium vanadium fluorophosphate, LiVPO[sub 4]F, J. Electrochem. Soc. 150 (2003) A1394.
[19] J. Barker, R.K.B. Gover, P. Burns, A. Bryan, M.Y. Saidi, J.L. Swoyer, Structural and

electrochemical properties of lithium vanadium fluorophosphate, $LiVPO_4F$, J. Power Sources 146 (2005) 516–520.
[20] R. Gover, P. Burns, A. Bryan, M. Saidi, J. Swoyer, J. Barker, $LiVPO_4F$: a new active material for safe lithium-ion batteries, Solid State Ion. 177 (2006) 2635–2638.
[21] Z. Liu, W. Peng, K. Shih, J. Wang, Z. Wang, H. Guo, G. Yan, X. Li, L. Song, A. MoS2, coating strategy to improve the comprehensive electrochemical performance of $LiVPO_4F$, J. Power Sources 315 (2016) 294–301.
[22] S. Zhong, Z. Yin, Z. Wang, Q. Chen, Synthesis and electrochemical properties of Al-doped $LiVPO_4F$ cathode materials for lithium-ion batteries, Rare Met. 26 (2007) 445–449.
[23] J. Wang, X. Li, Z. Wang, H. Guo, Y. Li, Z. He, B. Huang, Enhancement of electrochemical performance of Al-doped $LiVPO_4F$ using AlF_3 as aluminum source, J. Alloy. Compd. 581 (2013) 836–842.
[24] S. Zhong, F. Li, J. Liu, Y. Li, X. Deng, Preparation and electrochemical studies of Y-doped $LiVPO_4F$ cathode materials for lithium-ion batteries, J. Wuhan. Univ. Technol. -Mater. Sci. Ed. 24 (2009) 552–556.
[25] Z. Liu, Y. Fan, W. Peng, Z. Wang, H. Guo, X. Li, J. Wang, Mechanical activation assisted soft chemical synthesis of Na-doped lithium vanadium fluorophosphates with improved lithium storage properties, Ceram. Int. 41 (2015) 4267–4271.
[26] X. Sun, Y. Xu, G. Chen, P. Ding, X. Zheng, Titanium doped $LiVPO_4F$ cathode for lithium ion batteries, Solid State Ion. 268 (2014) 236–241.
[27] Y. Xie, H. Yu, T. Yi, Q. Wang, Q. Song, M. Lou, Y. Zhu, Thermodynamic stability and transport properties of tavorite $LiFeSO_4F$ as a cathode material for lithium-ion batteries, J. Mater. Chem. A 3 (2015) 19728–19737.
[28] R.B. Araujo, M.S. Islam, S. Chakraborty, R. Ahuja, Predicting electrochemical properties and ionic diffusion in $Na_{2+2x}Mn_{2-x}(SO_4)_3$: crafting a promising high voltage cathode material, J. Mater. Chem. A 4 (2016) 451–457.
[29] M.M. Islam, T. Bredow, Interstitial lithium diffusion pathways in γ-$LiAlO_2$: a computational study, J. Phys. Chem. Lett. 6 (2015) 4622–4626.
[30] T. Zhang, D. Li, Z. Tao, J. Chen, Understanding electrode materials of rechargeable lithium batteries via DFT calculations, Prog. Nat. Sci.: Mater. Int. 23 (2013) 256–272.
[31] K.B. John, P. Perdew, Matthias Ernzerhof, Generalized gradient approximation made simple, Phys. Rev. Lett. 77 (1996) 3865–3868.
[32] G. Kresse, Efficient iterative schemes for ab initio total-energy calculations using a plane-wave basis set, Physcal Rev. B 54 (1996) 169–186.
[33] R.C. Kari Laasonen, Changyol Lee, David Vanderbilt, Implementation of ultrasoft pseudo potentials in ab initio molecular dynamics, Phys. Rev. B 43 (1991) 6796.
[34] H.J. Monkhorst, J.D. Pack, Special points for Brillouin-zone integrations, Phys. Rev. B 13 (1976) 5188.
[35] S.H. Chen, Z.R. Xiao, Y.P. Liu, P.H. Lee, Y.K. Wang, First-principle calculation on nearly half-metallic antiferromagnetic behavior of double perovskites La_2VReO_6, J. Magn. Magn. Mater. 323 (2011) 175–178.
[36] S.Y. Chung, J.T. Bloking, Y.M. Chiang, Electronically conductive phospho-olivines as lithium storage electrodes, Nat. Mater. 1 (2002) 123–128.
[37] J. Xu, G. Chen, Effects of doping on the electronic properties of $LiFePO_4$: a first-principles investigation, Physica B: Condens. Matter 405 (2010) 803–807.
[38] Y.M. Tatsuya Nakamuraa, Mitsuharu Tabuchi, Yoshihiro Yamada, Structural and surface modifications of $LiFePO_4$ olivine particles and their electrochemical properties, J. Electrochem. Soc. 153 (2006) A1108–A1114.
[39] N.V. Kosova, E.T. Devyatkina, A.B. Slobodyuk, A.K. Gutakovskii, $LiVPO_4F/Li_3V_2(PO_4)_3$ nanostructured composite cathode materials prepared via mechanochemical way, J. Solid State Electrochem. 18 (2013) 1389–1399.
[40] R.J. Messinger, M. Ménétrier, E. Salager, A. Boulineau, M. Duttine, D. Carlier, J.-M. Ateba Mba, L. Croguennec, C. Masquelier, D. Massiot, M. Deschamps, Revealing defects in crystalline lithium-ion battery electrodes by solid-state NMR: applications to $LiVPO_4F$, Chem. Mater. 27 (2015) 5212–5221.
[41] N. Govind, M. Petersen, G. Fitzgerald, D. King-Smith, J. Andzelm, A generalized synchronous transit method for transition state location, Comput. Mater. Sci. 28 (2003) 250–258.
[42] N. Kuganathan, M.S. Islam, Li_2MnSiO_4 lithium battery material: atomic-scale study of defects, lithium mobility, and trivalent dopants, Chem. Mater. 21 (2009) 5196–5202.
[43] Z.S.K.T. Xin, H. Lu, First-principles study of electronic structure and electrochemical property for $LiVPO_4F$, Chin. J. Inorg. Chem. 27 (2011) 1065–1070.
[44] P. Zhang, D. Zhang, L. Huang, Q. Wei, M. Lin, X. Ren, First-principles study on the electronic structure of a $LiFePO_4$ (010) surface adsorbed with carbon, J. Alloy. Compd. 540 (2012) 121–126.
[45] G.D.P. Jeremy, K. Burdett, Sarah L. Price, Role of the crystal-field theory in determining the structures of spinels, J. Am. Chem. Soc. 104 (1982) 92–95.
[46] H. Gretarsson, J.P. Clancy, X. Liu, J.P. Hill, E. Bozin, Y. Singh, S. Manni, P. Gegenwart, J. Kim, A.H. Said, D. Casa, T. Gog, M.H. Upton, H.S. Kim, J. Yu, V. M. Katukuri, L. Hozoi, J. van den Brink, Y.J. Kim, Crystal-field splitting and correlation effect on the electronic structure of A_2IrO_3, Phys. Rev. Lett. 110 (2013) 076402.
[47] C. Ouyang, D. Wang, S. Shi, Z. Wang, H. Li, X. Huang, L. Chen, First principles study on $Na_xLi_{1-x}FePO_4$ as cathode material for rechargeable lithium, Chin. Phys. Lett. 23 (2006) 61–64.
[48] Y. Wang, Z. Feng, J. Chen, C. Zhang, X. Jin, J. Hu, First principles study on electronic properties and occupancy sites of molybdenum doped into $LiFePO_4$, Solid State Commun. 152 (2012) 1577–1580.
[49] S. Thinius, M.M.I., P. Heitjans, T. Bredow, Theoretical study of Li migration in lithium – graphite intercalation compounds with dispersion-corrected DFT methods, J. Phys. Chem. C. 118 (2014) 2273–2280.
[50] M. Nakayama, M. Kaneko, M. Wakihara, First-principles study of lithium ion migration in lithium transition metal oxides with spinel structure, Phys. Chem. Chem. Phys. 14 (2012) 13963–13970.
[51] L. Sebastian, J. Gopalakrishnan, Lithium ion mobility in metal oxides: a materials chemistry perspective Based on a lecture delivered at the international symposium "Materials for Energy: Batteries and Fuel Cells", J. Mater. Chem. 13 (2003) 433–441.
[52] R. Kutner, Chemical diffusion in the lattice gas of non-interacting particles, Phys. Lett. A 81 (1981) 239–240.
[53] G.C.A. Van der Ven, Lithium diffusion mechanisms in layered intercalation compounds, J. Power Sources 97–98 (2001) 529–531.
[54] G.H. Tim Mueller, Anubhav Jain, Gerbrand Ceder, Evaluation of tavorite-structured cathode materials for lithium-ion batteries using high-throughput computing, Chem. Mater. 23 (2011) 3854–3862.
[55] J. Rui, Ma, L. Shao, X. Lin, K. Wu, M. Shu, P. Li, N. Long, Y. Ren, Determination of lithium ion diffusion behaviors in tavorite $LiVPO_4F$ by galvanostatic intermittent titration technique, Ceram. Int. 40 (2014) 15113–15119.
[56] J. Wang, X. Li, Z. Wang, H. Guo, B. Huang, Z. Wang, G. Yan, Systematic investigation on determining chemical diffusion coefficients of lithium ion in $Li_{1+x}VPO_4F$ ($0 \leq x \leq 2$), J. Solid State Electrochem. 19 (2014) 153–160.